

Numerical analysis of the dissipative two-state system with the density-matrix Hilbert-space-reduction algorithm

Yoshihiro Nishiyama

Department of Physics, Faculty of Science, Okayama University, Okayama 700-8530, Japan

Received: date / Revised version: date

Abstract. Ground state of the dissipative two-state system is investigated by means of the Lanczos diagonalization method. We adopted the Hilbert-space-reduction scheme proposed by Zhang, Jeckelmann and White so as to reduce the overwhelming reservoir Hilbert space to being tractable in computers. Both the implementation of the algorithm and the precision applied for the present system are reported in detail. We evaluate the dynamical susceptibility (resolvent) with the continued-fraction-expansion formula. Through analysing the resolvent over a frequency range, whose range is often called ‘interesting’ frequency, we obtain the damping rate and the oscillation frequency. Our results agree with those of a recent quantum Monte-Carlo study, which concludes that the critical dissipation from oscillatory to over-damped behavior decreases as the tunneling amplitude is strengthened.

PACS. 75.40.Mg numerical simulation studies – 05.40.+j Fluctuation phenomena, random processes, and Brownian motion – 05.70.Ln Nonequilibrium thermodynamics, irreversible processes

1 Introduction

Effect of dissipation on quantum tunneling phenomenon lies out of the scope of the conventional weak coupling (Markovian) approximation, and has been studied extensively so far [1,2]. In order to introduce dissipation, Caldeira and Leggett [3,4] involved a thermal reservoir which consists of oscillators influencing stochastic (Brownian) fluctuations to the tunneling two-level system. Their model, the so-called spin-boson model, is given by the following Hamiltonian,

$$\mathcal{H} = -\frac{\Delta}{2}\sigma^x + \sum_{i=1}^N \omega_i a_i^\dagger a_i + \frac{\sigma^z}{2} \sum_{i=1}^N f_i (a_i^\dagger + a_i), \quad (1)$$

where the operators $\{\sigma^\alpha\}$ denote the Pauli operators and the operators a_i and a_i^\dagger denote the bosonic annihilation and creation operators, respectively, for the i -th oscillation mode ($i = 1 \sim N$). The set of these oscillators works as the above-mentioned reservoir with respect to the spin $1/2\sigma$. The coupling coefficients $\{f_i\}$ should be arranged so as to satisfy the so-called Ohmic-dissipation condition,

$$J(\omega) = \pi \sum_i f_i^2 \delta(\omega - \omega_i) \quad (2)$$

$$= \begin{cases} 2\pi\alpha\omega & (\omega \ll \omega_c) \\ 0 & (\omega \gg \omega_c) \end{cases}. \quad (3)$$

The dimensionless constant α controls the strength of the dissipation, and the cut-off frequency ω_c defines the energy

unit throughout this paper; $\omega_c = 1$. The transverse field Δ induces quantum coherence (tunneling amplitude) between the spin up-and-down states, whereas the coupling to the reservoir disturbs the coherence. These conflicting effects are the central concern of the problem, which are apparently non-perturbative in nature.

It is noteworthy that the spin-boson model (1) is equivalent to the anisotropic Kondo model [5,6,7,8]. The parameter α controls the strength of the longitudinal Kondo coupling, whereas Δ controls the transverse-coupling strength. Thereby, the region $\alpha < 1$ ($\alpha > 1$) is identified as the antiferromagnetic (ferromagnetic) Kondo phase; see the ground-state phase diagram shown in Fig. 1. That is, in

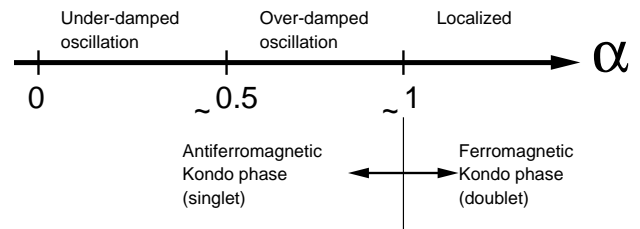


Fig. 1. The ground-state phase diagram of the spin-boson model (1) with the Ohmic dissipation. Quantitative estimation of the relaxation parameters such as the damping rate and the oscillation frequency is the main concern of this paper.

the region $\alpha < 1$, the up-and-down spin states form a coherent (singlet) state through a certain tunneling ampli-

tude, whereas in $\alpha > 1$, the tunneling amplitude vanishes owing to the dissipation [9,10]. Hence, in the region $\alpha > 1$, the ground state is degenerated doubly. The effective tunneling amplitude is found to vanish at the phase boundary in the form [11,12],

$$\Delta_{\text{eff}} = \Delta \left(\frac{\Delta}{\omega_c} \right)^{\frac{\alpha}{1-\alpha}}. \quad (4)$$

Owing to the equivalence, we readily investigate the equilibrium (thermodynamic) properties by means of various theoretical techniques which have been developed so far for the Kondo problem. Note, however, the dynamical (non-equilibrium) properties are rather out of the scope of these analytical techniques; refer to the paper [13] for a recent analytical approach. The dynamical properties, especially in the frequency range $\sim \Delta_{\text{eff}}$, are the very concern of the present topic. The noninteracting-blip approximation [2,14] was invented so as to describe the relaxation dynamics of this particular frequency range. This approximation is, however, justified in a rather limited parameter range $\alpha < 0.5$.

Hence, in order to investigate the relaxation properties, various numerical simulations have been performed so far. Chakravarty and Rudnick performed quantum Monte-Carlo simulation [15]; the model they simulated is a one-dimensional long-range Ising model, which was derived [16,17] through eliminating the reservoir (conduction electron) degrees of freedom. They succeeded in obtaining the spectral function through the Padé approximation of the imaginary time correlation function followed by the analytic continuation (Wick rotation). As a result, they found that the long-range asymptotic form of the dynamical correlation is governed by power law. This conclusion was supported by Strong [18] with use of the similar numerical technique. Völker [19] followed the Chakravarty-Rudnick analysis, and reported that ‘quasi-particle’ picture explains the spectral-function data. As a consequence, he obtained the damping rate and frequency. We utilize the picture to analyze our density-matrix-renormalization data. Costi and Kieffer [20,21] used the Wilson numerical renormalization technique to calculate the spectral function. Their technique is particularly useful in order to investigate the Kondo fixed-point (very low temperature) physics definitely. Time-evolution simulation was performed with use of stochastic sampling (path integral) algorithm [22]. The method has an advantage over others that one can observe real-time dynamics directly. The stochastic-sampling error, however, grows as the evolution time is lengthened.

In the present paper, for the first time, we perform Lanczos-diagonalization analysis of the spin-boson model (1). In order to command vast assembly of the reservoir-oscillator modes, we adopted the density-matrix truncation scheme proposed by Zhang, Jeckelmann and White [23]. (They studied the one-dimensional polaron system with this truncation technique.) The rest of this paper is organized as follows. In the next section, we propose an implementation of their algorithm to the spin-boson model (1), and report the precision in detail. In Section 3,

by means of this new technique, we investigate the relaxation properties of the spin-boson model. We evaluate the dynamical susceptibility (resolvent), which is readily calculated in our scheme with use of the continued-fraction-expansion formula [24,25]. Analyzing the analyticity of the resolvent, we confirm the above-mentioned ‘quasi particle’ picture [19] so as to obtain the damping rate and frequency. Our results are contrasted with the former quantum Monte-Carlo results [19]. In the last section, we give summary and discussions.

2 Application of the Hilbert-space-truncation algorithm to the spin-boson model

In this section, we propose a prescription for adopting the Hilbert-space-reduction method to the spin-boson model. We then demonstrate the precision of our new scheme.

2.1 Hilbert-space-reduction algorithm

Even a single oscillator (boson) spans infinite-dimensional Hilbert space. Therefore, in order to treat an oscillator with the exact diagonalization method, one must truncate the Hilbert space inevitably. In conventional simulations, the boson state is represented in terms of its occupation number, and those states whose occupation number exceeds a limit are disregarded (discarded). Zhang, Jeckelmann and White [23] proposed an alternative representation and a truncation criterion. Applying their scheme to a polaron system (one-dimensional Holstein model), they demonstrated that the scheme yields very precise results, although the dimensionality of each oscillator is reduced to three. This truncation is called ‘(numerical) renormalization.’ Their new bases are particularly efficient in those cases where the oscillator equilibrium position is shifted by a certain external force (coordinate-coordinate coupling). This is precisely the case of the present model (1).

In the following, we explain the detail how we adopt their algorithm to the spin-boson model. First, we limit the Hilbert-space dimensionality of each oscillator to d dimensions except an oscillator with D dimensions; see Fig. 2. We call the d -dimensional oscillators ‘small oscillators,’ and the D -dimensional one ‘big oscillator.’ The choice of the big oscillator is to be made in sequence among the various reservoir oscillator modes ($\alpha = 1 \sim N$). The sequence is continued until the relevant bases, explained below, become converged. In our experience, a few sweeps are sufficient for the convergence. The space of each small oscillator is spanned by the above-mentioned truncated relevant bases, and thus the creation and the annihilation operators should be represented in terms of these bases correspondingly. (Before renormalization, the space is allowed to be of the number representation ($|n\rangle$, $n = 1 \sim d-1$), and the operators are expressed in terms of this subspace.) On the other hand, the space of the big oscillator is spanned by the occupation-number representation with $n = 0 \sim D-1$. From this D -dimensional space, d relevant bases are renormalized (extracted) in the following manner.

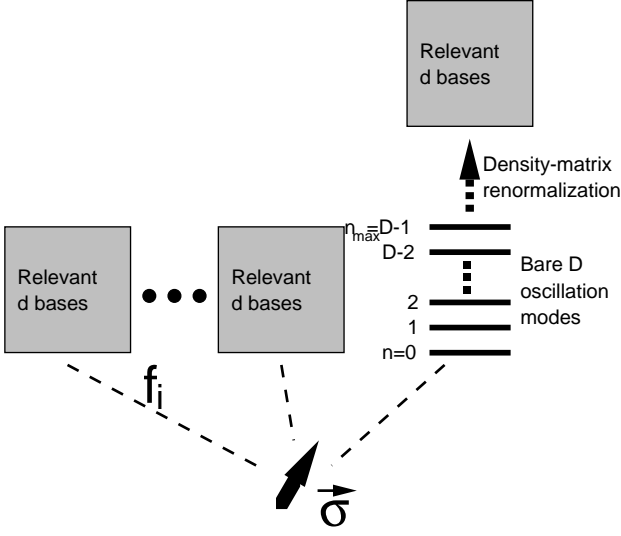


Fig. 2. Schematic drawing of the density-matrix-renormalization algorithm applied to the spin-boson model (1).

Second, we diagonalize the Hamiltonian (1) with the Lanczos technique to obtain the ground state $|\Psi_0\rangle$. Note that the Hamiltonian consists of the operators whose matrix elements are already prepared in the above. The ground-state vector should be represented in the form,

$$|\Psi_0\rangle = \sum_{i,j} \psi_{ij} |i\rangle_A |j\rangle_B, \quad (5)$$

where the bases $\{|i\rangle_A\}$ are of the big site, and the bases $\{|j\rangle_B\}$ are of the remaining part of the system. Thereby, we construct the (reduced) density matrix subjected to the big oscillator,

$$\rho_{ii'} = \sum_j \psi_{ij} \psi_{i'j}^*. \quad (6)$$

The new bases $\{\mathbf{u}^\beta\}$ are determined so as to diagonalize the density matrix,

$$\rho \mathbf{u}^\beta = w_\beta \mathbf{u}^\beta. \quad (7)$$

According to the proposal [26,27], the new relevant bases (subspace) should be spanned by the eigenvectors \mathbf{u}^β up to the d -th largest weight (eigenvalue) w_β . That is, the new annihilation operator of the big oscillator is re-represented in terms of these d relevant eigenvectors in the following manner,

$$[\tilde{b}_i]_{\beta\beta'} = {}^t \mathbf{u}^\beta b_i \mathbf{u}^{\beta'}. \quad (8)$$

Because the renormalization is subjected to the reduced density matrix, the renormalization is called ‘density matrix’ renormalization [26,27].

The renormalization is continued for every oscillator modes ($i = 1 \sim N$) successively until the relevant bases become fixed (converged). In our experience, a few sweeps are sufficient for the convergence.

Finally, we mention how we chose the frequencies $\{\omega_\alpha\}$ and the coupling constants $\{f_i\}$. The choice is arbitrary under the constraint eq. (3). We have uniformly distributed the oscillator frequency over the range $0 < \omega < \omega_c (= 1)$, and determined the coupling constants so as to satisfy the constraint. We numbered the oscillator modes ($\alpha = 1 \sim N$) in order of the frequency ω_α (from the slowest to the fastest).

2.2 Precision of the Hilbert-space-truncation algorithm

In this subsection, we show the precision of the algorithm explained in the preceding subsection. In Fig. 3, we plotted the transverse magnetization $\langle \sigma^x \rangle$ for the system $N = 8$, $\Delta = 0.3$ and $\alpha = 0.5$ by means of the conventional truncation scheme; namely, the boson states are represented in term of the occupation number, and the occupation number is restricted within $n \leq n_{\max}$. (Note

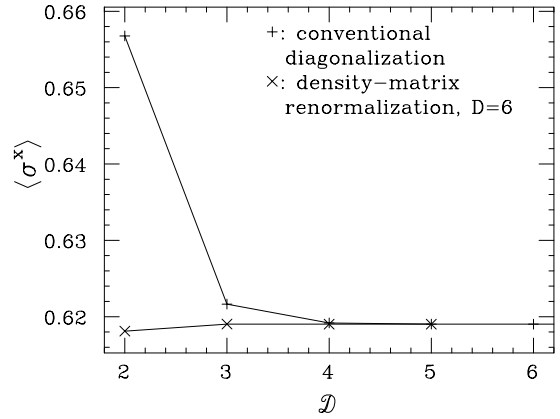


Fig. 3. The transverse magnetization is plotted for the system with $N = 8$, $\Delta = 0.3$ and $\alpha = 0.5$ with the dimensionality \mathcal{D} of each oscillator varied. The plots + are evaluated with the conventional occupation-number representation. The occupation number is restricted within $n \leq n_{\max}$. Hence, $\mathcal{D} = n_{\max} + 1$. The plots x are those evaluated with the density-matrix-truncation algorithm. The dimensionality of each small oscillator d is varied ($\mathcal{D} = d$) with the big oscillator dimensionality fixed ($D = 6$).

that the transverse magnetization indicates a degree to what extent the tunneling is disturbed by the reservoir fluctuations.) Hence, the dimensionality of each oscillator is given by $\mathcal{D} = n_{\max} + 1$. We observe that through increasing \mathcal{D} , the results converge to a certain limit. In the same plot, we show the results by means of the density-matrix-renormalization method for the same system as the above ($N = 8$, $\Delta = 0.3$ and $\alpha = 0.5$). In this renormalization, we fixed the dimensionality of the big oscillator as $D = 6$, and varied the small-oscillator dimensionality d ; hence, $\mathcal{D} = d$. We see that, with fewer number of bases,

the renormalization results converge more rapidly than the former occupation-number-representation results. As is mentioned in the previous subsection, the equilibrium position of each oscillator is shifted by the coordinate-coordinate coupling. The relevant bases of the density-matrix renormalization are constructed so as to take into account of the fluctuations from the equilibrium position, whereas the occupation-number bases are rather inefficient to represent these shifted oscillator modes.

In Fig. 4, we show the relative error of the transverse magnetization of the density-matrix-renormalization method ($D = 6$); the error is defined as the deviation from the the conventional occupation-number-truncation diagonalization with $\mathcal{D} = n_{\max} + 1 = 6$. The system parameters are the same as those shown in Fig. 3. We observe,

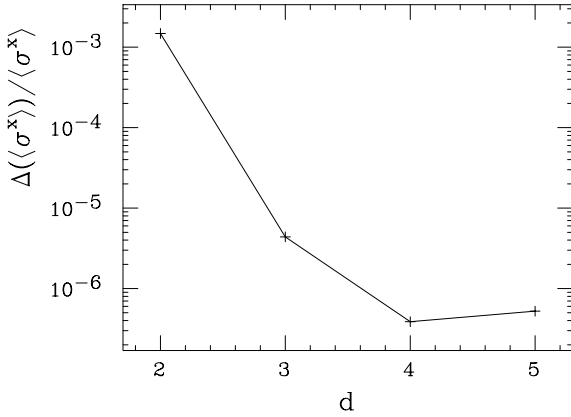


Fig. 4. The relative error of the transverse magnetization with the density-matrix-renormalization method. We varied the number of remained bases d with $D = 6$ fixed. The system parameters are the same as those shown in Fig. 3.

with very limited number of relevant bases ($d = 2 \sim 3$), the density-matrix renormalization reproduces the full-diagonalization result precisely. The relative error is saturated to $\sim 10^{-7}$ due to the numerical round-off error for $d \geq 4$. The result indicates that a few relevant oscillator modes are of importance. In Fig. 5, we show the weight w_β of each eigenstate ($i = 1 \sim D$) for each reservoir oscillator ($\alpha = 1 \sim N$). The weight w_β indicates the statistical weight of the state \mathbf{u}^β contributing to the ground state. We notice that, in fact, the first few bases are particularly weighted, and the other states are irrelevant ($w_\beta < 10^{-5}$), and to be ignored. Furthermore, it should be noted that these features are common to all the reservoir modes ($i = 1 \sim N$).

To summarize, in Fig. 3, we found that by means of the conventional occupation-number truncation, the result converges gradually as the occupation-number threshold n_{\max} is increased. We see that the occupation numbers exceeding $n \approx 6$ are hardly excited. In the density-matrix renormalization, see Figs. 4-5, we found that only the first

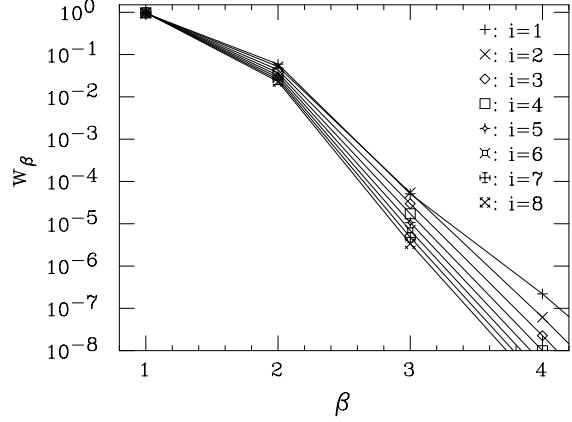


Fig. 5. The weight w^β (density-matrix eigenvalue) is plotted for each oscillator mode ($i = 1 \sim 8$).

few states are particularly weighted. Hence, hereafter, we set the dimension of the big site to be $D = 6$, and remain two relevant states ($d = 2$) for each oscillator mode. We believe that the number of the reservoir oscillators is prior to the number of remained bases d for each mode: Note that as the number of the reservoir modes is increased, the coupling constants $\{f_i\}$ should be reduced correspondingly; the oscillators become less disturbed. In the following, we simulate the reservoir consisting of eighteen oscillator modes. Hence, the truncation error is expected to be reduced furthermore from those shown in this subsection.

3 Density-matrix-renormalization analysis of the dissipative tunneling

With use of the method developed in the preceeding section, we investigate the relaxation properties in the ground state of the spin boson model (1). These properties are extracted from the dynamical susceptibility, which is readily evaluated in our scheme. Our results of the relaxation coefficients are contrasted with those obtained by means of the quantum Monte-Carlo simulation [19].

3.1 Dynamic susceptibility — continued-fraction-expansion formula

In this subsection, we evaluate the dynamical susceptibility, and compare ours with that obtained at an integrable point $\alpha = 0.5$. The analyticity of the susceptibility is analyzed extensively in the next subsection so as to yield relaxation properties.

Linear response theory states that the relaxation (non-equilibrium) process should be described in term of a certain ground-state equilibrium dynamical correlation function, unless the process is not so far from equilibrium.

In other words, equilibrium dynamical correlation function does contain informations about non-equilibrium processes. For that purpose, we calculated the following dynamical susceptibility,

$$\begin{aligned}\chi''(\omega) &= \frac{1}{2} \int_{-\infty}^{\infty} dt e^{i\omega t} \langle [\sigma^z(t), \sigma^z] \rangle \\ &= \text{Im} \left(\left\langle \sigma^z \frac{1}{\omega + E_g - \mathcal{H} + i\eta} \sigma^z \right\rangle \right. \\ &\quad \left. - \left\langle \sigma^z \frac{1}{\omega - E_g + \mathcal{H} - i\eta} \sigma^z \right\rangle \right) \quad (9) \\ &= \text{Im} G(\omega). \quad (10)\end{aligned}$$

Some might wonder that the inverse matrix of the total Hamiltonian appearing in eq. (9) cannot be computed; this is true. The *expectation value* of the inverse of the Hamiltonian is, however, evaluated with use of the Gagliano-Balestro continued-fraction formula [24,25],

$$\left\langle f_0 \left| \frac{1}{z - \mathcal{H}} \right| f_0 \right\rangle = \frac{\langle f_0 | f_0 \rangle}{z - \alpha_0 - \frac{\beta_1^2}{z - \alpha_1 - \frac{\beta_2^2}{z - \alpha_2 - \frac{\beta_3^2}{\ddots}}}}, \quad (11)$$

where the coefficients are given by the Lanczos tri-diagonal elements,

$$\begin{aligned}|f_{i+1}\rangle &= \mathcal{H}|f_i\rangle - \alpha_i|f_i\rangle - \beta_i^2|f_{i-1}\rangle, \quad (12) \\ \alpha_i &= \langle f_i | \mathcal{H} | f_i \rangle / \langle f_i | f_i \rangle, \\ \beta_i^2 &= \langle f_i | f_i \rangle / \langle f_{i-1} | f_{i-1} \rangle \quad (\beta_0 = 0).\end{aligned}$$

Therefore, through choosing of the Lanczos initial vector as $|f_0\rangle = \sigma^z |\Psi_0\rangle$, we readily evaluate the dynamical susceptibility by means of the same numerical procedure used in the preceding Lanczos diagonalization.

We expanded the formula (11) up to the one-hundredth order. This is comparable with the iteration number needed to obtain the low-lying states in the Lanczos diagonalization. Therefore, the expansion is expected to yield precise result concerning low-lying frequencies. This frequency range is sufficient for our purpose, because we are concerned in the frequency range $\sim \Delta_{\text{eff}}$. Moreover, in practice, at high frequencies, the magnitude of the spectral intensity is suppressed considerably.

In Fig. 6, we plotted the spectral function,

$$S(\omega) = \frac{\chi''(\omega)}{\omega}, \quad (13)$$

for the parameters $\Delta = 0.2$, $\alpha = 0.5$ and $N = 18$. (The spectral function is related closely to the linear-response function.) At the point $\alpha = 0.5$, the Hamiltonian (1) is reduced to being quadratic through a canonical transformation, and the spectral intensity is calculated exactly in the form [12],

$$\begin{aligned}S(\omega) &= \frac{8\tilde{\Delta}^2}{\pi} \frac{1}{\omega^2 + 4\tilde{\Delta}^2} \\ &\quad \times \left(\frac{1}{\omega\tilde{\Delta}} \arctan\left(\frac{\omega}{\tilde{\Delta}}\right) + \frac{1}{\omega^2} \ln\left(1 + \frac{\omega^2}{\tilde{\Delta}^2}\right) \right) \quad (14)\end{aligned}$$

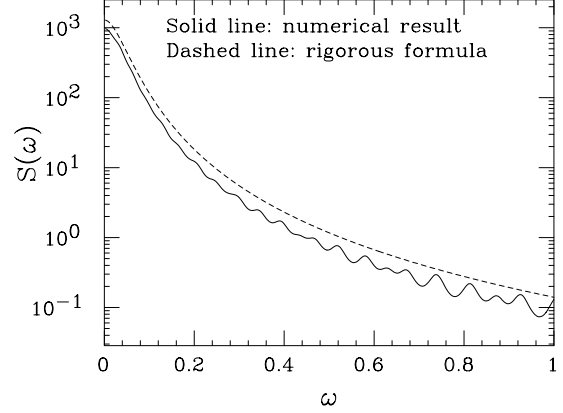


Fig. 6. The spectral function $S(\omega)$ (13) is plotted for $\Delta = 0.2$ and $\alpha = 0.5$. The solid line is our density-matrix-renormalization result for $N = 18$. The delta-function peaks are broadened into the Lorentz form with the width $\eta = 0.022$. The dashed line shows a rigorous result (14), which is available at the Toulouse point $\alpha = 0.5$.

($\tilde{\Delta} = (\pi/4)\Delta^2/\omega_c$). The rigorous result is plotted in Fig. 6 as well. We observe that our numerical data reproduces the rigorous formula. The slight difference may be attributed to the spectral form (3) of the reservoir around the cut-off frequency. We used a non-analytic reservoir spectrum which vanishes suddenly at the cut-off frequency. This difference may become irrelevant, if the tunneling amplitude is set to be sufficiently small compared with the cut-off frequency.

3.2 Analyticity of the dynamical susceptibility (resolvent) and the damping properties

In this subsection, we investigate the analyticity of the dynamical susceptibility (9), from which we extract informations about relaxation properties. In Fig. 7, we plotted the imaginary-time correlation function,

$$\mathcal{G}(i\omega) = - \int_0^\beta d\tau \langle e^{\tau\mathcal{H}} \sigma^z e^{-\tau\mathcal{H}} \sigma^z \rangle_\beta e^{i\omega\tau} \quad (15)$$

$$= G(i\omega) \quad (\beta \rightarrow \infty), \quad (16)$$

for the system with $\Delta = 0.2$, $\alpha = 0.2$ and $N = 18$. As is shown in the plot, the numerical result is fitted well by the ‘quasi-particle’ formula,

$$\mathcal{G}(i\omega) = \frac{A}{(\omega + \lambda)^2 + \tilde{\omega}^2}. \quad (17)$$

This fact was pointed out by Völker, who performed a quantum Monte-Carlo simulation; see Introduction. As is apparent from the definition (9), the (fitting) parameters λ and $\tilde{\omega}$ give the damping rate and the frequency, respectively, of the ‘coordinate’ σ^z perturbed from the equilibrium position. According to the formula (17), the following

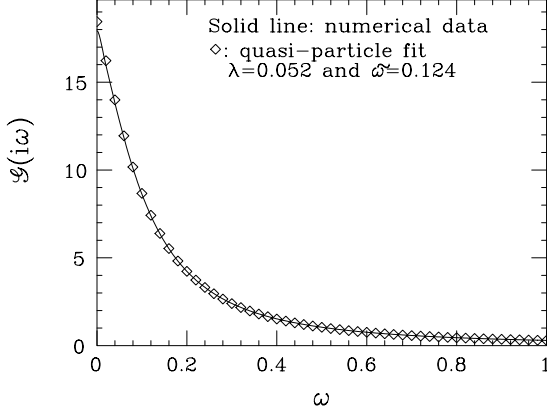


Fig. 7. The imaginary-time Green function (15) is plotted for $N = 18$, $\Delta = 0.2$ and $\alpha = 0.2$. The solid line is our density-matrix-renormalization result. The plots \diamond are those of the ‘quasi-particle’ form (17) with the damping coefficients $\lambda = 0.052$ and $\tilde{\omega} = 0.124$.

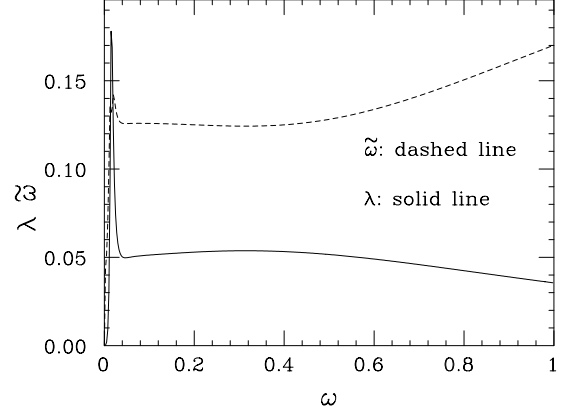


Fig. 8. The damping coefficients λ (18) and $\tilde{\omega}$ (19) are plotted; the system parameters are the same as those in Fig. 7. Around the frequency range $\sim \Delta_{\text{eff}} (\approx 0.13)$, these quantities remain invariant, indicating that over this range of time, the dynamics is described by the quasi-particle picture (17).

relations hold;

$$\lambda = \frac{\frac{d}{d\omega} (\mathcal{G}(i\omega))^{-1}}{\frac{d^2}{d\omega^2} (\mathcal{G}(i\omega))^{-1}} - \omega, \quad (18)$$

$$\tilde{\omega} = \sqrt{\frac{2(\mathcal{G}(i\omega))^{-1}}{\frac{d^2}{d\omega^2} (\mathcal{G}(i\omega))^{-1}} - (\omega + \lambda)^2}. \quad (19)$$

From these relations, we estimate the damping coefficients λ and $\tilde{\omega}$. It is one of the advantages of our scheme that one can differentiate the function $\mathcal{G}(i\omega)$, because it is expanded in the analytic form (11). In Fig. 8, we plotted the right hand side of eqs. (18) and (19); the system parameters are the same as those in Fig. 7. We see that these quantities are invariant actually over a certain frequency range $\sim \Delta_{\text{eff}} (\approx 0.13)$, and thus the quasi-particle picture (17) holds in the time range $\sim \Delta_{\text{eff}}^{-1}$. As is explained in Introduction, we are concerned in the physics of this particular range of time. In consequence, we obtained the poles of $G(\omega)$ at $\omega = \pm\tilde{\omega} - i\lambda$, which are *away* from the real axis. It is noteworthy that such irreversible features are not transparent in the original high-order-expansion result (11). Through the above data analysis, such the relaxation features become clear; we discuss this point afterwards.

In Fig. 9, we plotted the damping rate and the frequency. These damping coefficients are estimated both with the procedure as is shown in Fig. 8 and with the conventional least square fit by the function (17). Our results of the density-matrix renormalization confirm the former quantum Monte-Carlo study [19]: The oscillation frequency $\tilde{\omega}$ is suppressed as the dissipation is strengthened. It vanishes around $\alpha \approx 0.5$. This point indicates the transition between the under-damped and the over-damped oscillations. By means of the bosonization technique [8], this transition point was predicted to locate at

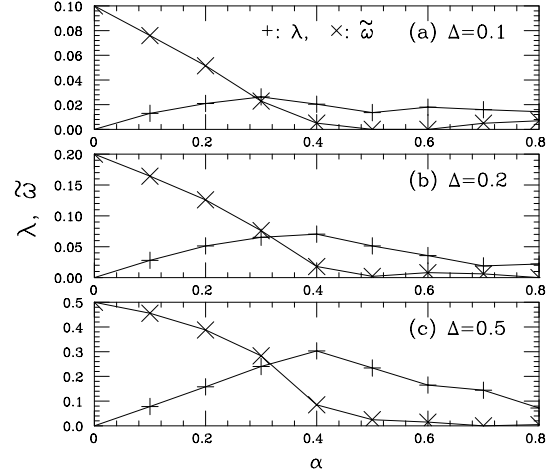


Fig. 9. The damping rate λ and the frequency $\tilde{\omega}$ estimated by means of the density-matrix-renormalization algorithm; (a) $\Delta = 0.1$, (b) $\Delta = 0.2$ and (c) $\Delta = 0.5$. These are to be contrasted with those of quantum Monte-Carlo method [19].

$\alpha = 0.5$ irrespective of the tunneling amplitude strength Δ . Because in the bosonization technique, the band width (cut-off frequency) is supposed to be sufficiently large compared with the many-body interactions (Δ and α), the validity in the strong-coupling region is not necessarily assured. In Fig. 9, in fact, we see that the $\tilde{\omega}$ plots become curved convexly, as the tunneling amplitude is strengthened, and accordingly it becomes evident that the transition point locates below $\alpha = 0.5$. These features were reported in the paper [19], and were suspected to be due to a systematic numerical error caused by the critical slowing down. In our diagonalization calculation, we are free from

the critical slowing down. Therefore, we conclude that for larger values of Δ , the transition point actually shifts below $\alpha = 0.5$. Furthermore, we confirm the report [19] that at $\alpha = 1/3$, the damping rate and the frequency coincide. At this point, the peaks around $\omega = \pm\tilde{\omega}$ of spectral intensity (13) merge into a single peak so that this point was suspected to indicate a certain phase transition. The present result suggests that the point is merely the situation where the damping feature smears out the oscillatory behaviour, because these relative strengths exchange.

We see that in Fig. 9 (a) ($\Delta = 0.1$), the plots for $\alpha > 0.6$ are rather scattered (irregular). In that region, the quasi-particle poles shift towards the origin of the complex plane ($\pm\tilde{\omega} - \lambda \rightarrow 0$), so that the dumping parameters degenerate into the slowest reservoir oscillation mode. In that situation, our method becomes inapplicable. Similar difficulty arises in the vicinity of the localization transition point $\alpha = 1$ for larger values of Δ .

We are in a position to discuss the above quasi-particle feature furthermore in detail. It is noteworthy that the form (17) implies that the analyticity of the dynamical susceptibility is broken along the real axis; the upper and lower complex planes are not continued analytically. This is precisely due to the reservoir effect, which drives the spin state to be in equilibrium, violating the time-reversal symmetry. In our numerical result, however, the upper and the lower complex planes are continued analytically, although along the real axis, there distribute vast number of poles densely. This feature contradicts the above quasi-particle picture insisting isolated poles at $\omega = \pm\tilde{\omega} - i\lambda$. This inconsistency is simply due to the fact that our reservoir spectrum is not continuous, and thus the time-reversal symmetry is maintained. Only through the limit of infinite oscillator modes, these poles merge into the ‘quasi-particle’ poles away from the real axis. Hence, in order to extract relaxation properties, one should avoid the real axis, along which the result is suffered significantly from discontinuity of the reservoir modes. Along the imaginary axis, as is shown in Fig. 7, the result is smooth and monotonic, and is much easier to be fitted by the quasi-particle form. That is why we examined the imaginary-time Green function (15) just as Völker did for analyzing his Monte-Carlo data computed at each Matsubara frequency. We stress that our resolvent is evaluated (expanded) in the analytical (continued-fraction) form as in eq. (11). Therefore, as is shown previously in Fig. 6, one can obtain the spectral function (real-time Green function) immediately through performing the Wick rotation. This is one of the advantages of the present scheme over others.

4 Summary and discussions

We investigated the dissipative two-state system (1) through applying the density-matrix Hilbert-space-truncation algorithm [23]. An implementation of this algorithm is proposed, and the precision applied to the present model is reported in detail. We found that in our situation where the

oscillator equilibrium position is shifted by the coordinate-coordinate coupling, the density-matrix renormalization works much better than the conventional occupation-number-truncation method. We have remained two relevant states for each oscillator mode, so that we succeeded in treating eighteen oscillators, keeping the truncation error considerably small. We believe that the number of tractable oscillators is more crucial in observing the relaxation properties than the ‘quality’ (fidelity) of each oscillator mode. In fact, we reproduced the dynamical susceptibility at the Toulouse point $\alpha = 0.5$, at which a rigorous formula is known. We stress that, in our scheme, the susceptibility is evaluated in the *analytical* continued-fraction form (11), which is apparently advantageous over others in performing the analytic continuation (Wick rotation); in order to observe relaxation (time irreversible) properties from numerical data, which apparently possesses the time-reversal symmetry, we need to examine the analyticity of the resolvent (dynamical susceptibility); see Section 3.2. In fact, after the immediate analytic continuation to the imaginary axis, we found that the result is well fitted by the form (17), confirming Völker’s finding [19] with quantum Monte-Carlo method. That is, the susceptibility possesses the so-called quasi-particle poles away from the real axis $\omega = \pm\tilde{\omega} - i\lambda$. In consequence, we obtained the damping rate λ and the frequency $\tilde{\omega}$. Both agree with those of the quantum Monte-Carlo method [19]. In particular, our results confirm the former report that for larger values of Δ , the transition point between the over-damped and the under-damped oscillations shifts downwards ($\alpha_c < 0.5$). For studying such critical property, our method is advantageous over the Monte-Carlo method, because our method is free from the critical slowing down.

Acknowledgement

Our program is based on the subroutine package TIT-PACK ver. 2 coded by professor H. Nishimori.

References

1. A. O. Caldeira and A. J. Leggett: Ann. Phys. **149** (1983) 374; **153** (1984) 445(E).
2. A. J. Leggett, S. Chakravarty, A. T. Dorsey, M. P. A. Fisher, A. Garg and W. Zwerger: Rev. Mod. Phys. **59** (1987) 1; **67** (1995) 725(E).
3. A. O. Caldeira and A. J. Leggett: Phys. Rev. Lett. **46** (1981) 211; **48** (1982) 1571.
4. A. O. Caldeira and A. J. Leggett: Physica **121A** (1983) 587; **130A** (1985) 374(E).
5. S. Chakravarty: Phys. Rev. Lett. **49** (1982) 681.
6. A. J. Bray and M. A. Moore: Phys. Rev. Lett. **49** (1982) 1545.
7. V. Hakim, A. Muramatsu and F. Guinea: Phys. Rev. B **30** (1984) 464.
8. F. Guinea, V. Hakim and A. Muramatsu: Phys. Rev. B **32** (1985) 4410.
9. B. De Raedt and H. De Raedt: Phys. Rev. Lett. **50** (1983) 1926.

10. B. De Raedt and H. De Raedt: Phys. Rev. B **29** (1984) 5325.
11. F. Guinea, V. Hakim and A. Muramatsu: Phys. Rev. Lett. **54** (1985) 263.
12. F. Guinea: Phys. Rev. B **32** (1985) 4486.
13. F. Lesage, H. Saleur and S. Skorik: Phys. Rev. Lett. **76** (1996) 3388.
14. S. Chakravarty and A. J. Leggett: Phys. Rev. Lett. **52** (1984) 5.
15. S. Chakravarty and J. Rudnick: Phys. Rev. Lett. **75** (1995) 501.
16. P. W. Anderson, G. Yuval and D. R. Hamann: Phys. Rev. B **1** (1970) 4464.
17. P. W. Anderson and G. Yuval: J. Phys. C **4** (1971) 607.
18. S. P. Strong: Phys. Rev. E **55** (1997) 6636.
19. K. Völker: Phys. Rev. B **58** (1998) 1862.
20. T. A. Costi and C. Kieffer: Phys. Rev. Lett. **76** (1996) 1683.
21. T. A. Costi: Phys. Rev. B **55** (1997) 3003.
22. J. T. Stockburger and C. H. Mak: Phys. Rev. Lett. **80** (1998) 2657.
23. C. Zhang, E. Jeckelmann and S. R. White: Phys. Rev. Lett. **80** (1998) 2661.
24. E. R. Gagliano and C. A. Balseiro: Phys. Rev. Lett. **59** (1987) 2999.
25. E. R. Gagliano and C. A. Balseiro: Phys. Rev. B **38** (1988) 11766.
26. S. R. White: Phys. Rev. Lett. **69** (1992) 2863.
27. S. R. White: Phys. Rev. B **48** (1993) 10345.